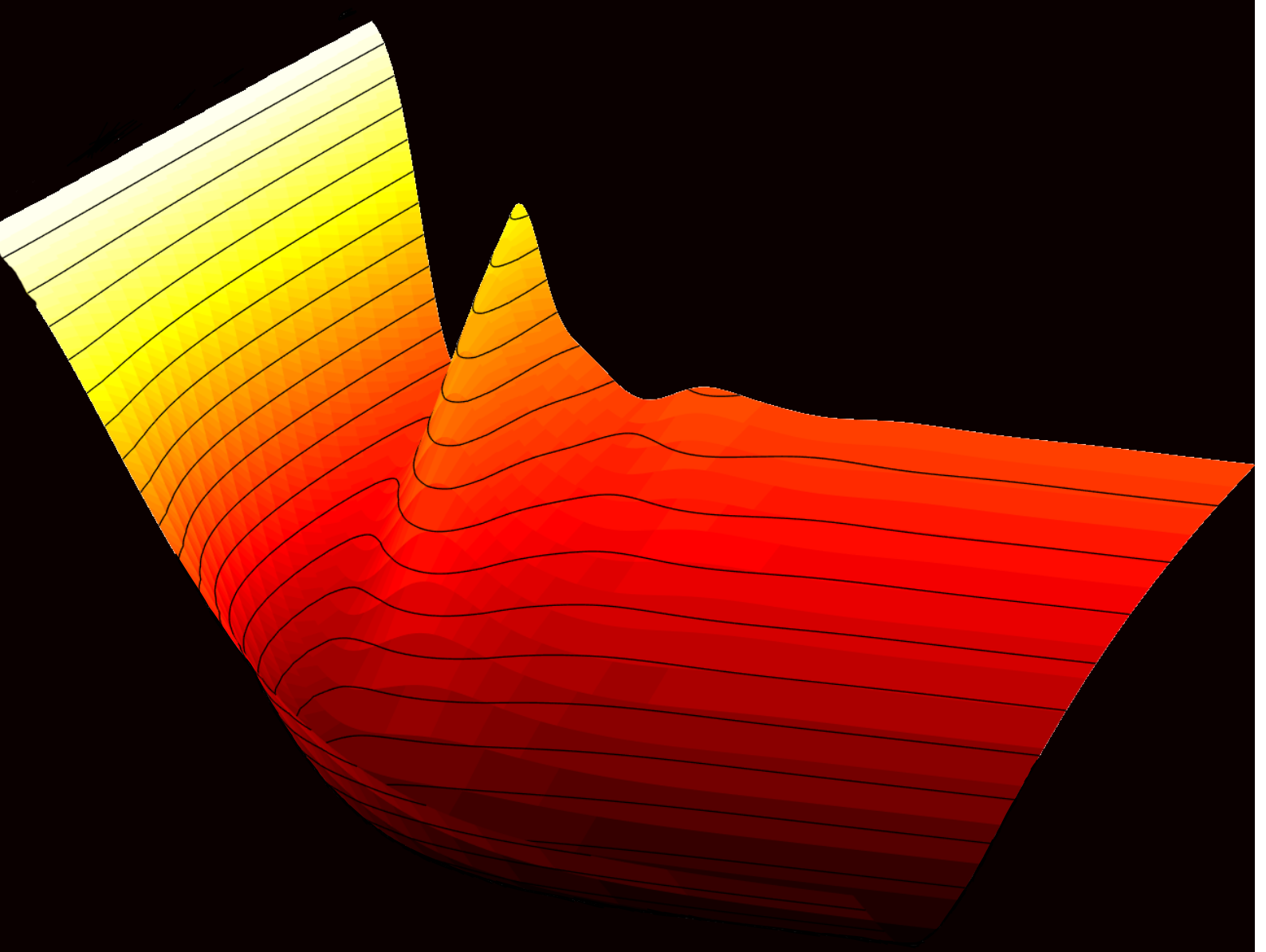

Kerr Resonator

Oliver Gordon & Matthew Edmondson

Image: 3D contour plot of time evolution of second order coherence function for a Kerr resonator

Abstract

By varying the initial parameters of a pumped Kerr non-linear oscillator, a wide range of long-term behaviours can be found. These behaviours can be exploited by allowing the creation of quantum switches, transistors, and random number generators in superconducting circuits. In this investigation, we derive a semi-classical approximation of the average number of photons in a non-linear oscillator. We also derive a set of coupled equations of motion for the reduced density operator describing the system, before using MATLAB to numerically calculate the long-term behaviour of the system as we vary the pumping strength, non-linearity and frequency difference between the pump and the oscillator. By looking at various parameters and comparing the numerical to the semi-classical approximation, we find that varying parameters of the system in turn results in very different effects on the long-term evolution of the system.

Contents

1 Introduction

Kerr non-linear media have recently seen significant attention as a means to investigate quantum mechanical phenomena. As discovered in 1875 by John Kerr[1], when an electric field is applied to a Kerr medium its refractive index will change in proportion to the field. As this effect is non-linear, quantum oscillators can be formed by driving a resonator containing a Kerr medium with an external pump. These systems have been shown to contain many interesting quantum dynamical properties[2].

As a consequence of strong non-linearity, the way in which these non-linear oscillators evolve over time strongly depends on their initial parameters and environment. For example, completely different behaviours are seen when an otherwise identical system is subject to specific driving pulses, rather than the continuous pumping used here[3]. As such, understanding exactly how initial parameters affect long-time behaviour is critical to improving the performance of many systems based on Kerr non-linear oscillators. Besides the wide range of applications of Kerr media to optical systems[4], Kerr oscillators are often used in quantum switches[5,6], photon blockades[3], and random number generators[7]. However, these areas of interest have only begun to be investigated recently.

In this investigation, we begin by deriving an equation of motion for the expectation value of the lowering operator, a, $\langle \dot{a} \rangle$. We then make a semi-classical approximation to introduce the complex amplitude, α, and therefore derive an equation cubic in $|\alpha|^2$. From here, we derive a set of coupled equations of motion for the density operator of the system in matrix form, $\dot{\rho}_{n,n'}$. After initially considering a system beginning in the vacuum state, we then use MATLAB to numerically perform a 45^{th} order Runge-Kutta integration until the system settles into a steady state. This enables us to investigate the mixing of the system, $\mathrm{Tr}[\rho^2]$, the average number of photons in the system, $\langle a^\dagger a \rangle$, and the second-order coherence, $g^{(2)}(0)$, in the long-timescale limit. We also compare $\langle a^\dagger a \rangle$ when calculated either numerically or with the semi-classical approximation.

2 Theory & Methods

In order to computationally investigate a Kerr non-linear resonator subjected to an external drive, we first consider a system that is modelled by a Hamiltonian of the form,

$$H = \hbar\Delta_\rho a^\dagger a + \frac{\hbar K}{2} a^\dagger a^\dagger a a + i\hbar\epsilon_\rho \left(a^\dagger - a\right), \qquad \{1\}$$

where Δ_ρ is the difference in frequency between the quantum oscillator and the pump driving it. ϵ_ρ describes the strength of the pump, whilst K describes the strength of the non-linearity of the system.

The reduced density operator of the system can be formed by taking into account the coupling of the system to its environment. This results in the equation of motion of the reduced density operator, $\dot{\rho}(t)$, being given by,

$$\dot{\rho}(t) = \frac{d\rho(t)}{dt} = -\frac{i}{\hbar}\left[H, \rho(t)\right] - \frac{\kappa}{2}\left(a^\dagger a\rho(t) - 2a\rho(t)a^\dagger + \rho(t)a^\dagger a\right), \qquad \{2\}$$

where κ describes the coupling of the system to the environment.

2.1 Semi-Classical Approximation

To make a semi-classical approximation of the oscillator, we first calculate the equation of motion of the expectation value of the lowering operator, a, $\langle\dot{a}\rangle$. As derived in Appendix A.1, by calculating the trace of $a\dot{\rho}$, we arrive at the equation,

$$\langle\dot{a}\rangle = -i\Delta_\rho\langle a\rangle - iK\langle a^\dagger a a\rangle - \frac{\kappa}{2}\langle a\rangle + \epsilon_\rho. \qquad \{3\}$$

From here, we can define the complex amplitude $\alpha = \langle a\rangle$. We can then make a semi-classical approximation by changing the expectation value of the product of the operators to the product of the expectation values of the operators. For example, $\langle a^\dagger a a\rangle \Rightarrow \langle a^\dagger\rangle\langle a\rangle\langle a\rangle \Rightarrow |\alpha|^2\alpha$.

As derived in Appendix A.2, we can set the time derivative of Equation 3 to 0 and therefore form an equation cubic in $|\alpha|^2$, as given by the equation,

$$K^2|\alpha|^6 + 2K\Delta_\rho|\alpha|^4 + \left(\frac{\kappa^2}{4} + \Delta_\rho^2\right)|\alpha|^2 - \epsilon_\rho^2 = 0. \qquad \{4\}$$

As there is no time dependence in this equation, the approximation is only valid for long-timescale behaviours of our density operator. As α is a complex amplitude, we therefore expect $|\alpha|^2$ to be real, and as such do not consider the imaginary roots of this equation. Instead, we take the smallest fully real solution. This solution was calculated numerically using MATLAB.

2.2 Coupled Equations of Motion

Next, we act on Equation 2 on the left side with $\langle n|$ and on the right with $|n'\rangle$. By writing the density operator as a matrix in terms of the number states n and n', we can produce a set of coupled equations of motion for each matrix element n and n'. A detailed derivation can be found in Appendix A.3. Each matrix element of the equation of motion of the density operator, $\dot{\rho}_{n,n'}(t)$, is related to each matrix element of the density operator, $\rho_{n,n'}(t)$, by the equation,

$$\begin{aligned}\dot{\rho}_{n,n'}(t) = \langle n|\dot{\rho}|n'\rangle = \rho_{n,n'}(t)\Big[i\Delta_\rho(n'-n) + \frac{iK}{2}\big(n'(n'-1) - n(n-1)\big) - \frac{\kappa}{2}(n+n')\Big] \\ + \rho_{n-1,n'}(t)\Big[\epsilon_\rho\sqrt{n}\Big] - \rho_{n+1,n'}(t)\Big[\epsilon_\rho\sqrt{n+1}\Big] \\ + \rho_{n,n'-1}(t)\Big[\epsilon_\rho\sqrt{n'}\Big] - \rho_{n,n'+1}(t)\Big[\epsilon_\rho\sqrt{n'+1}\Big] \\ + \rho_{n+1,n'+1}(t)\Big[\kappa\sqrt{n+1}\sqrt{n'+1}\Big].\end{aligned} \quad \{5\}$$

As the evolution of the system is dependant on its initial state, the density matrix at zero time must be specified. This allows a matrix of $\dot{\rho}(0)$ to be calculated using Equation 5. Typically, we set the density matrix to be the vacuum state $\rho(0) = |0\rangle\langle 0|$. Using MATLAB, $\dot{\rho}(t)$ can then be numerically integrated with a 45$^{\text{th}}$ order Runge-Kutta differential solver until the system reaches a steady state. At this point, the system is at its long-time limit.

2.3 Extracting Parameters

At each time step calculated by the Runge-Kutta differential solver, several parameters can be extracted. To determine Tr[$\rho(t)$], the sum of the diagonals of each matrix of $\rho(t)$ is calculated. To ensure that the system is physical, the trace of the density operator should equal 1 since it represents the sum of the probabilities of the system being in any particular state. The degree to which the system is mixed is also considered through the calculation of Tr[$\rho(t)^2$]. The trace of ρ^2 ranges from 0 to 1, where a pure, linear system has Tr[$\rho(t)^2$] = 1, while decreasing values indicate an increasing mixing of states.

The average number of photons in the oscillator, $\langle a^\dagger a\rangle$ is determined by multiplying ρ by the matrix forms of the raising and lowering operators, and calculating the trace of the resulting matrix. This number can be compared to the solution of the semi-classical approximation made for Equation 4 in the long-time limit, since $|\alpha|^2 \equiv \langle a^\dagger\rangle\langle a\rangle = \langle a^\dagger a\rangle$.

Finally, the 2$^{\text{nd}}$ order coherence $g^{(2)}(0)$ can be calculated by the same method as the average number of photons. This coherence function is described by $g^{(2)}(0) = \langle a^\dagger a^\dagger a a\rangle / \langle a^\dagger a\rangle^2$, and for a system to be described classically[8], $g^{(2)}(0) = 1$. This would be the case at all times if we were to make the semi-classical approximation used in Section 2.1. If $g^{(2)}(0) < 1$, the system is non-linear, and exhibits sub-poissonian statistics than can only be explained quantum mechanically[9]. This demonstrates the particle-like nature of the photons. Meanwhile, if $g^{(2)}(0) > 1$, then the statistics of the system are super-poissonian.

3 Results

3.1 Initial Parameters & Demonstrating Accuracy

For typical input values of $\Delta_\rho = 0$, $\epsilon_\rho/\kappa = 1$, $K/\kappa = -0.5$, and a simulation size of 25x25, each of these four quantities were plotted against time in Figure 1. For all calculations in this investigation, we set $\kappa = 1$.

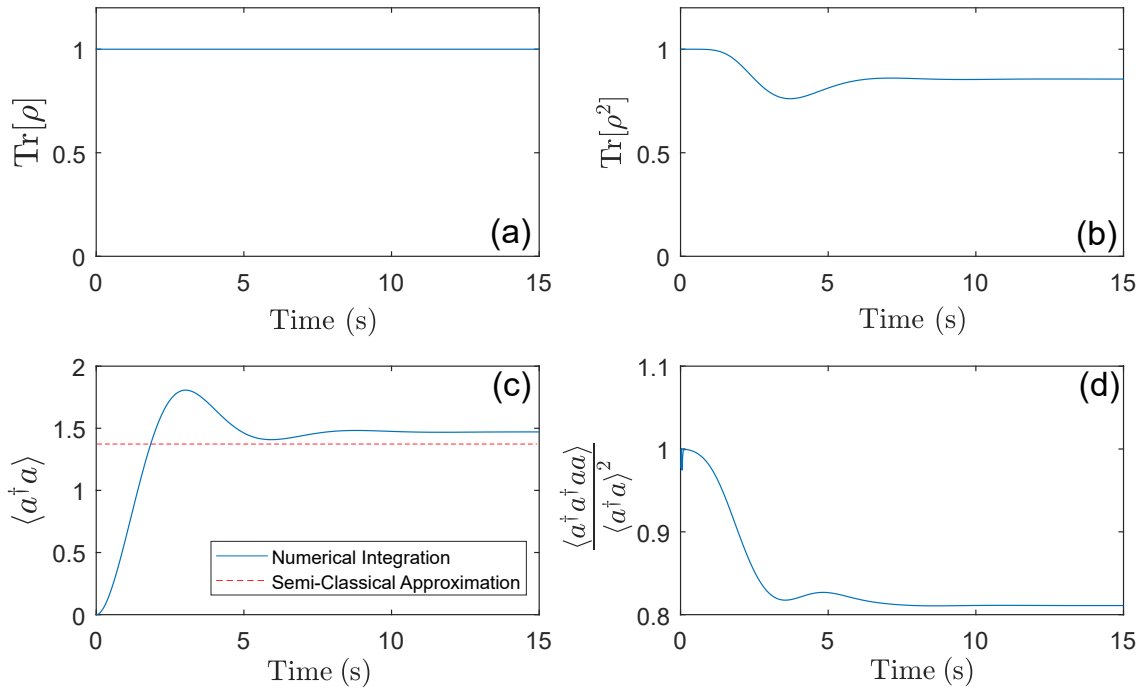

Figure 1: The time evolution of a pumped Kerr oscillator, for (a) Tr[ρ], (b) degree of mixing of states, (c) average number of photons inside the oscillator, and (d) second-order coherence function. Initially, the system is in a vacuum state with $\Delta_\rho = 0$, $\epsilon_\rho/\kappa = 1$ and $K/\kappa = -0.5$. As expected, we find Tr[ρ] = 1 for all times. In all cases, it can also be seen that the system settles into a stable state after approximately 10 seconds.

From Figure 1, we see that the system consistently settled into stable, long-timescale behaviour by 10 seconds. As such, we recorded long-timescale values at 15 seconds. Furthermore, we found $\mathrm{Tr}[\rho]$ to equal 1 to floating point precision for all timescales. This is expected behaviour, as $\mathrm{Tr}[\rho]$ is a summation of the probabilities of occupying different states, and a complete set of probabilities should sum to 1. We also found that 0 photons were initially in the oscillator, as expected. Furthermore, $\mathrm{Tr}[\rho^2] = 1$, which indicated that the system began in a pure, unmixed state. This was in agreement with the finding that $g^{(2)}(0) = 1$, which provided another calculation finding that the system was initially linear. This was expected, as the system was initially placed in the linear vacuum state.

After oscillating and entering the long-time limit, the system became mixed with $\mathrm{Tr}[\rho^2] = 0.86$. This was understandable, as the energy levels in this system were non-linear, and there were 1.47 photons present on average in the oscillator to allow this mixing to take place. This is seen in Figure 1(c). Because the coherence of the system dropped below 1, to $g^{(2)}(0) = 0.81$, the system was not fully classical, making the semi-classical approximation not fully valid. This resulted in a small discrepancy in the calculation of photons present, with the semi-classical approximation underestimating by 6%, at 1.38 to 1.47.

We also tested the fully linear case where $K = 0$, with all other parameters remaining as in Figure 1. As shown in Figure 2, we found that for the fully linear case, $\mathrm{Tr}[\rho^2] = 1$ for all times, indicating that the system remained pure and unmixed, as expected. It was also seen that $g^{(2)}(0) = 1$ for all times, indicating that the system was always in a fully coherent state, which is to be expected for a linear system. Furthermore, as $g^{(2)}(0) = 1$, the semi-classical approximation should hold well. Indeed, we found this to be the case, with the calculated average number of photons in the oscillator agreeing with the approximation to 5 decimal places.

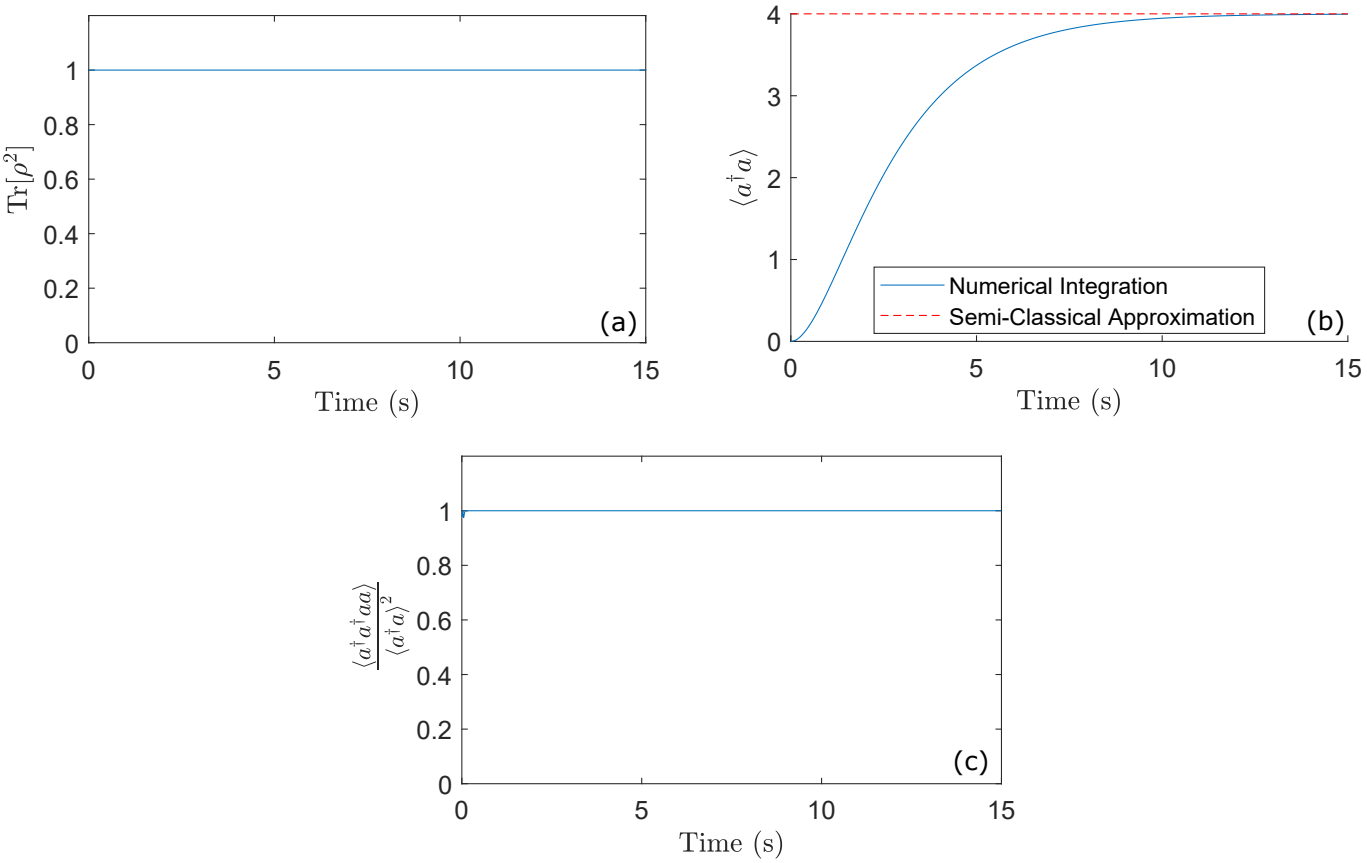

Figure 2: Figure to demonstrate the validity of numerical integration code written to model a driven non-linear Kerr oscillator. From initial values of $\Delta_\rho = 0$, $\epsilon_\rho/\kappa = 1$, the non-linearity of the system, K/κ, was set to 0, creating a fully linear system. As expected, this resulted in an unmixed, pure system, as indicated by (a) $\mathrm{Tr}[\rho^2] = 1$ and (c) $g^{(2)}(0) = 1$ for all timescales. As seen in (b) there is also a high degree of agreement with the semi-classical approximation used to model the system for the average number of photons in the oscillator, as expected for this linear case.

Furthermore, the case of zero pumping strength where $\epsilon_\rho/\kappa = 0$ was also considered, with all other parameters remaining as in Figure 1. This is shown in Figure 3. As expected, we found that no photons were present in the oscillator at any time, resulting in $\langle a^\dagger a\rangle = 0$. This was in agreement with the semi-classical approximation to floating point precision. Furthermore, no mixing occurred when no photons were present for obvious reasons, and as expected we found $\mathrm{Tr}[\rho^2] = 1$ for all times.

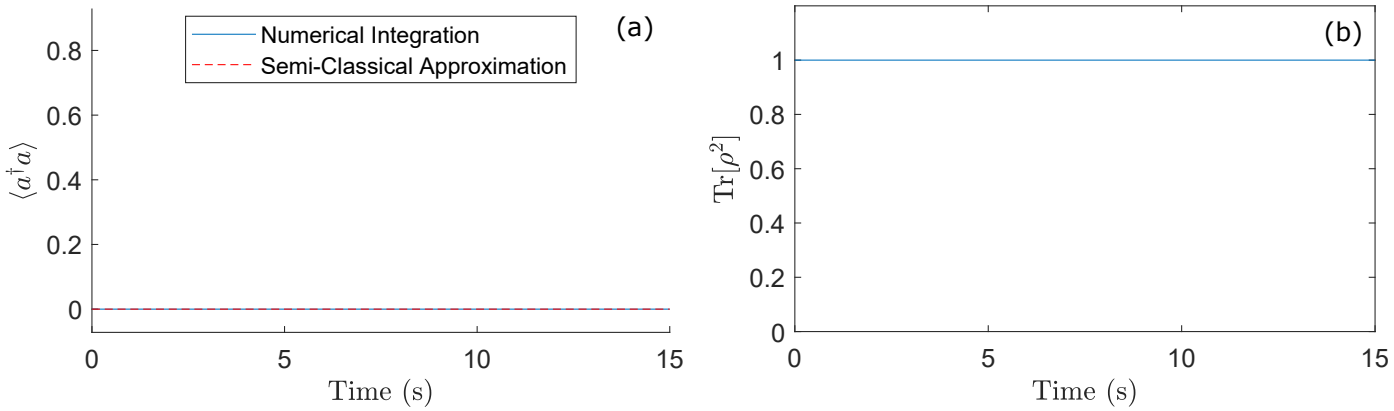

Figure 3: Figure to demonstrate the validity of numerical integration code written to model a driven non-linear Kerr oscillator. From initial values of $\Delta_\rho = 0$, $K/\kappa = -0.5$, the driving strength, ϵ_ρ/κ, was set to 0. This resulted in no photons being present in the oscillator, as seen in (a), and the system therefore remaining in a fully pure state, as seen in (b), for all times.

We also considered how simulation size affected accuracy. To allow numerical integration to take place in a reasonable amount of time, the n by n' matrices of $\rho(t)$ and $\dot{\rho}(t)$ were limited to the arbitrarily selected size of 25x25. This simulation size was chosen as for matrices larger than 10x10, no variation in the evolution of the system was seen, despite increasing the number of computations performed. This is demonstrated in Figure 4.

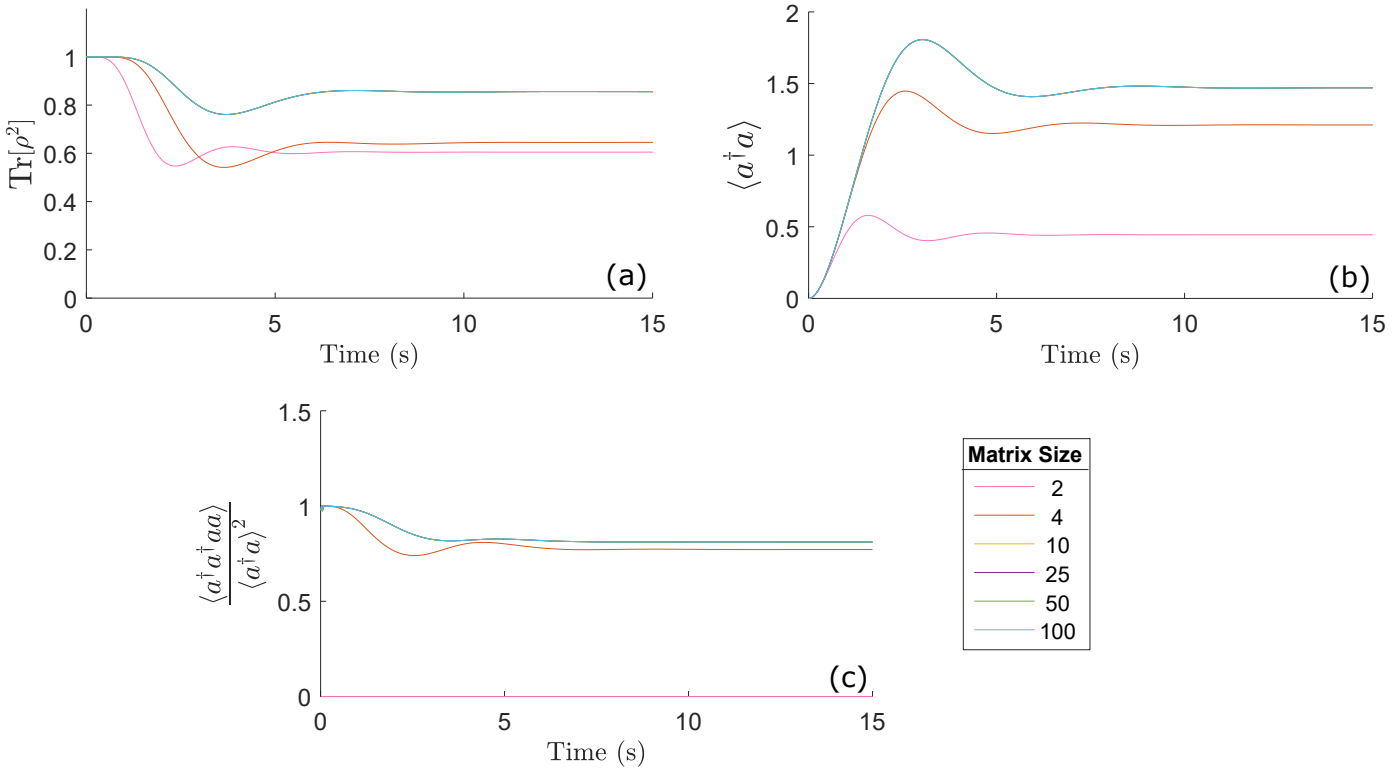

Figure 4: Figure to demonstrate the approximation of system size used to numerically integrate a driven non-linear Kerr oscillator. For a system initially in the vacuum state with $\Delta_\rho = 0$, $\epsilon_\rho/\kappa = 1$, $K/\kappa = -0.5$, the evolution of (a) $\mathrm{Tr}[\rho^2]$, (b) average number of photons in the oscillator, and (c) second-order coherence, was calculated for simulation sizes from 2x2 to 100x100. As it can be seen in all figures, identical results were seen for simulation sizes of above 10. We therefore performed all calculations for systems of size 25x25.

3.2 Exploring Long-Term Behaviour

3.2.1 Varying Starting Conditions

To explore long term behaviour, we first set $\Delta_\rho = 0$, $\epsilon_\rho/\kappa = 1$ and $K/\kappa = -0.5$ and varied the initial state of the system from $\rho(0) = |0\rangle\langle 0|$ to $\rho(0) = |1\rangle\langle 1|$, $\rho(0) = |5\rangle\langle 5|$ and $\rho(0) = |10\rangle\langle 10|$. For linear states, only one single diagonal term could be altered at a time, such that Tr[ρ] remained equal to 1. We found that for different initial states, the evolution of Tr[ρ], Tr[ρ^2], $\langle a^\dagger a\rangle$ and $g^{(2)}(0)$ remained identical to the $\rho(0) = |0\rangle\langle 0|$ case to floating point accuracy. However, we did not consider starting states that were mixed such as $\frac{1}{2}(|1\rangle\langle 1| + |2\rangle\langle 2|)$.

3.2.2 Varying K

Beginning with the linear case of K/κ=0, the dependence of long term behaviour on the non-linearity of the system was investigated. For initial values of $\Delta_\rho = 0$ and $\epsilon_\rho/\kappa = 1$, Figure 5 demonstrates the effect of changing K.

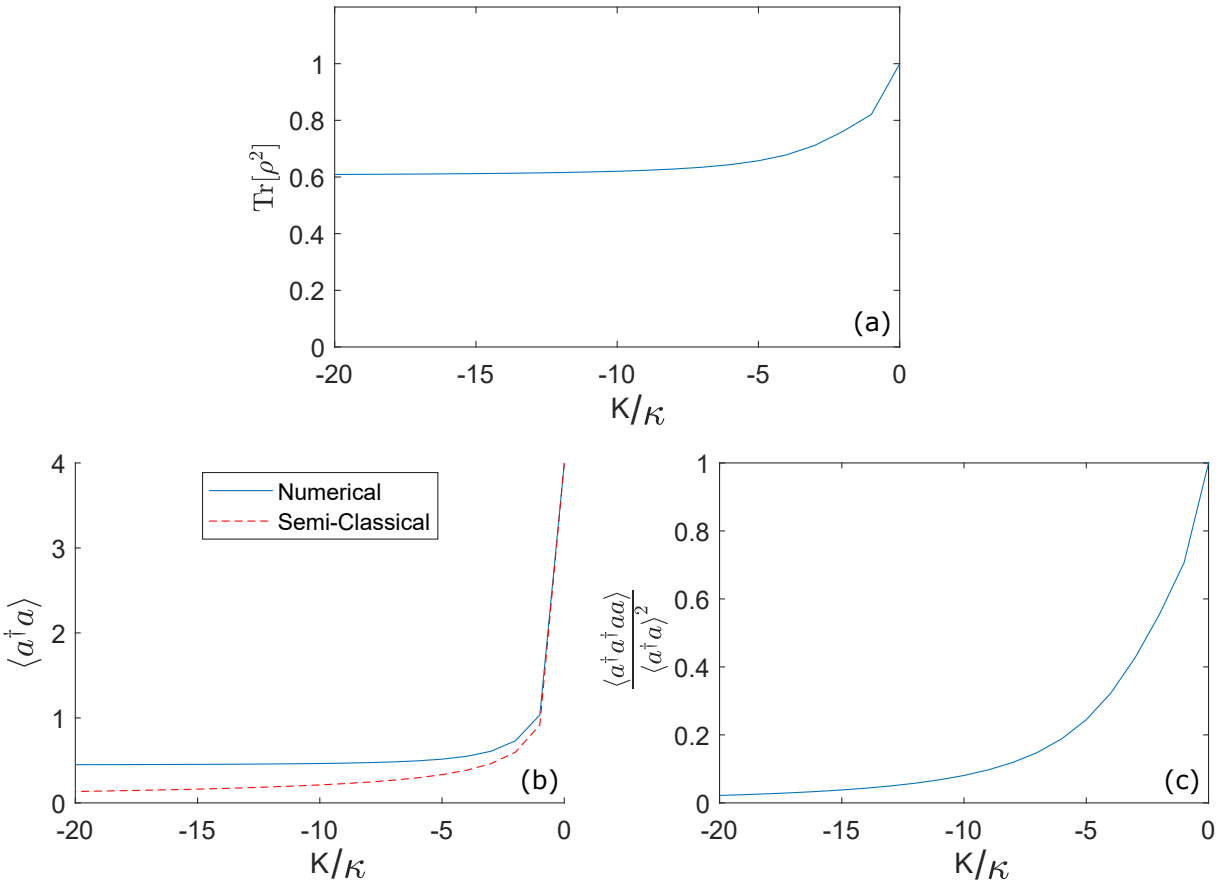

Figure 5: Figure to demonstrate the how the variation of K changes the long term solution of the system for initial values of $\Delta_\rho = 0$, $\epsilon_\rho = 1/\kappa$. For a system initially in the vacuum state, the values of (a) how mixed a state is Tr[ρ^2] for a given K, (b) the average number of photons, $\langle a^\dagger a\rangle$ as a function of K, and (c) the second-order coherence as a function of K. All data was run on a 25x25 matrix.

As seen in Figure 5(a), Tr[ρ^2] = 1 for $K = 0$, as at this point the system was fully linear. When the system became increasingly non-linear, the degree of mixing increased, and remained mixed for $K/\kappa < 0$. However, the degree of mixing plateaued for $K/\kappa <$ -10 to Tr[ρ^2] = 0.6, indicating that the system was more sensitive to initial parameters for low K. If a high degree of variation in long

term parameters is required, such as in the case of a random number generator, K should therefore be kept small.

Also, it can be seen from Figure 5(b) that there was a high degree of agreement between the semi-classical approximation and the numerical calculation for low non-linearity. However, as K decreased the approximation became increasingly less valid. This is explained by Figure 5(c), where it was seen that the coherence decreased further below 1 as K decreased. This explains the divergence, as below $g^{(2)}(0) = 1$, the system became less classical. The coherence also changed in a similar fashion to how $\langle a^\dagger a \rangle$ evolved. Furthermore, Figure 5(b) demonstrates that for decreasing values of K, decreasing numbers of photons became present in the oscillator in a similar fashion to the mixing of states. For applications where many photons are desired in an oscillator (such as a photon trap), it is therefore imperative to keep K small.

3.2.3 Varying ϵ_ρ

After varying K, we fixed $K/\kappa = -1$, set $\Delta_\rho = 0$ as before, and varied ϵ_ρ/κ from 0 to 20. Beginning with the same initial state of $\rho(0) = |0\rangle\langle 0|$, the effect of the pumping strength on long term behaviour is shown in Figure 6.

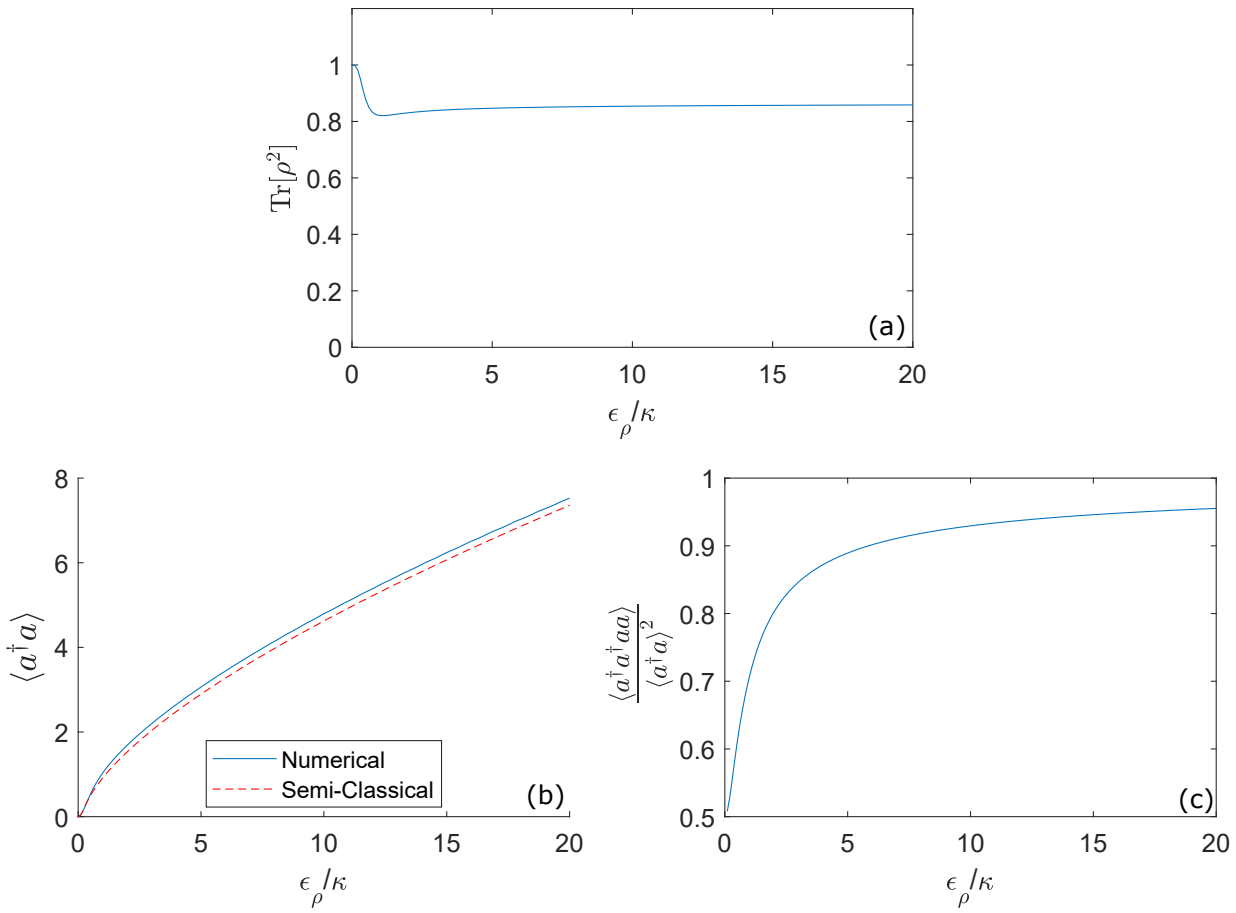

Figure 6: Figure to demonstrate the how the variation of ϵ_ρ/κ changes the long term solution of the system for initial values of $\Delta_\rho = 0$, $K\kappa = -1$. For a system initially in the vacuum state, the values of (a) how mixed a state is $\mathrm{Tr}[\rho^2]$ for a given ϵ_ρ/κ, (b) the average number of photons, $\langle a^\dagger a \rangle$ as a function of ϵ_ρ/κ, and (c) the second-order coherence as a function of ϵ_ρ/κ. All data was run on a 25x25 matrix.

At $\epsilon_\rho/\kappa = 0$, where there was no pumping, we found $\mathrm{Tr}[\rho^2] = 1$, indicating that the system was in a pure state. This was expected, as Figure 6(b) demonstrates that there were no photons in the oscillator in this case. As ϵ_ρ/κ increased, the system became increasingly mixed, but only as far as $\mathrm{Tr}[\rho^2] = 0.82$. As such, increasing pumping strength is therefore not a good method of increasing the mixing of states. Using Figure 6(b), we found that as the pumping increased, the number of photons increased near linearly. This indicated that increasing the pumping provided a simple and consistent means of increasing photon density in the oscillator across a wide range of pumping strengths.

It can also be seen from Figure 6 that the numerical and semi-classical solutions always agreed closely, with percentage error decreasing for higher $g^{(2)}(0)$. Similarly to the variation of K/κ, the semi-classical approach always underestimated the average number of photons present. The coherence function also always stayed below 1. However, it was not possible to describe a coherence function at $\epsilon_\rho/\kappa = 0$, as the denominator $\langle a^\dagger a\rangle$ was equal to zero at this point. It was, however, found that the system converged to $g^{(2)}(0) = 0.5$ in the limit of $\epsilon_\rho/\kappa = 0$.

3.2.4 Varying Δ_ρ

Finally, we fixed K/κ = -1, and $\epsilon_\rho/\kappa = 1$. For Δ_ρ varying from -20 to 20, the resulting data is plotted in Figure 7.

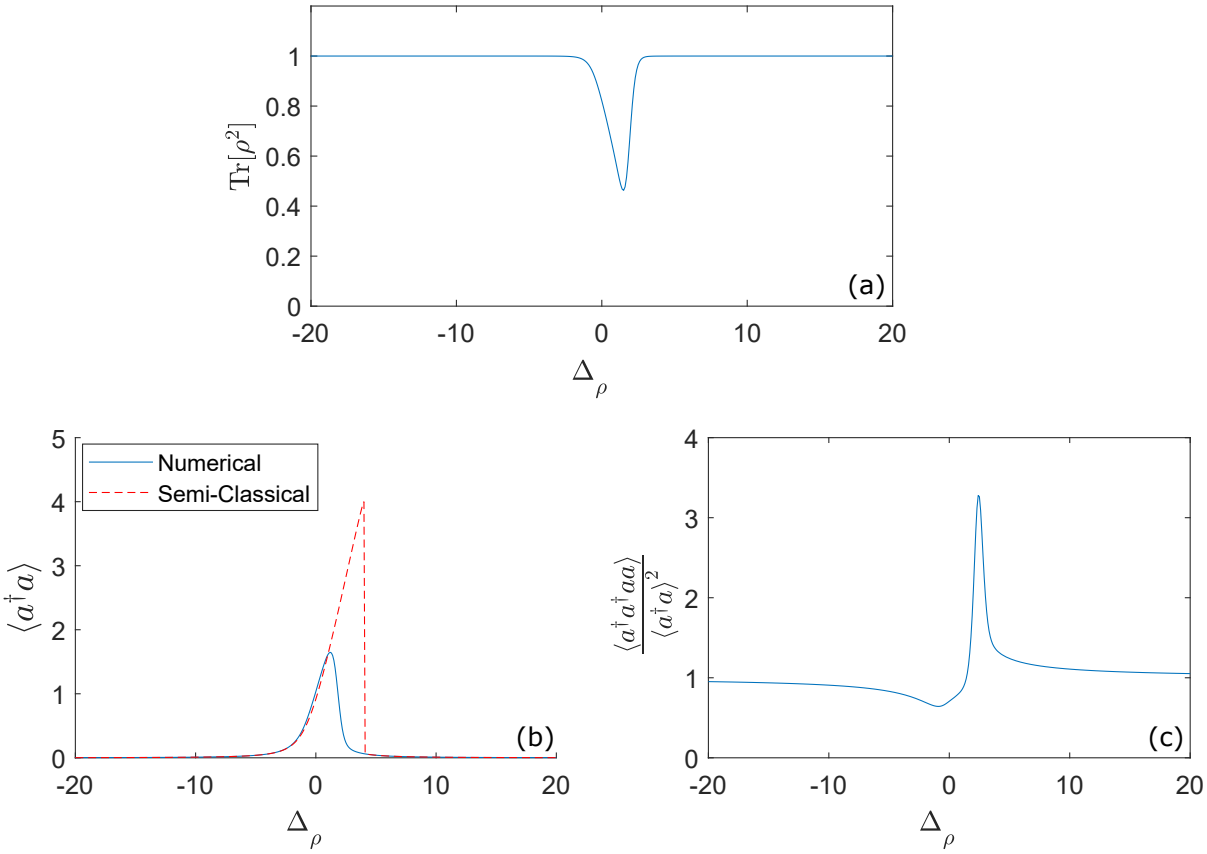

Figure 7: Figure to demonstrate the how the variation of Δ_ρ changes the long term solution of the system for initial values of $\epsilon_\rho/\kappa = 1$, $K/\kappa = -1$. For a system initially in the vacuum state, the values of (a) how mixed a state is $\mathrm{Tr}[\rho^2]$ for a given Δ_ρ, (b) the average number of photons, $\langle a^\dagger a\rangle$ as a function of Δ_ρ, and (c) the second-order coherence as a function of Δ_ρ. All data was run on a 25x25 matrix.

It can be seen in Figure 7(a) that the system remained in a pure state, except for a small range of values around $\Delta_\rho = 0$. Only in this small range did photons enter the material. This was understandable, as resonance should only occur if the driving frequency closely matches the natural oscillation frequency of the resonator. All other driving frequencies should be strongly damped. However, it was interesting to notice that this behaviour was asymmetric about $\Delta_\rho = 0$, with $\langle a^\dagger a \rangle$ showing a resonance peak at $\Delta_\rho = 1$. There was also a strong difference between the numerical and semi-classical solutions in resonant range, with the semi-classical solution following the rough shape of $g^{(2)}(0)$ in this area. For the non-resonant range of Δ_ρ, there was strong agreement of up to 6 decimal places.

To further investigate the resonant area, we considered how the number of the photons in the oscillator varied as a function of Δ_ρ for different K/κ values, as shown in Figure 8.

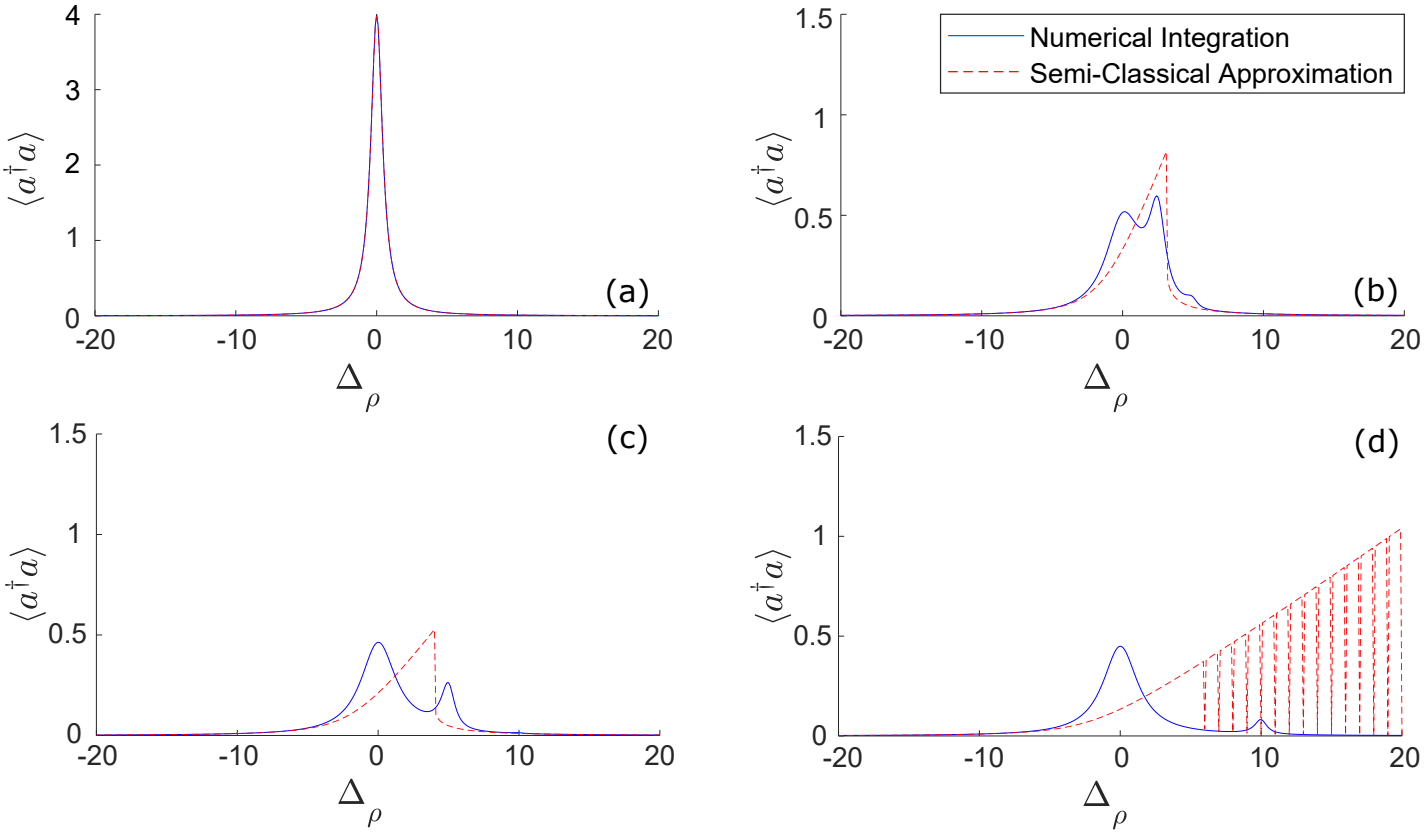

Figure 8: Figure to demonstrate how the effect of a differing K value impacts the numerical and semi-classical approximation for the average number of photons in the oscillator as a function of Δ_ρ. The values used are, (a) $K/\kappa = 0$, (b) $K/\kappa =$ -5, (c) $K/\kappa =$ -10, and (d) $K/\kappa =$ -20.

From these graphs, we found that as K/κ became more non-linear, a second resonance peak began to appear. Although the first peak was always seen at $\Delta_\rho = 0$ (which is different to the $K/\kappa = -1$ case) the second peak moved to increasingly higher values of Δ_ρ. Furthermore, a small third peak was also visible in Figure 8(b). As such, there may be a third peak present in Figures 8(c) and 8(d). This could be investigated further in future by increasing the range of Δ_ρ, and making peaks more prominent by increasing $\langle a^\dagger a \rangle$ by increasing ϵ_ρ/κ.

These observations were in agreement with work done by Shahinyan et al. in 2016, who noted[9] that with the exception of weak pumping strength, resonant peaks in photon population appear due to oscillatory Ramen processes. They also noted that these resonant frequencies are shifted due to Stark effects, with the shift increasing with K. However, we did not investigate the strength of this behaviour with higher pumping strengths.

Furthermore, the semi-classical approximation always began by agreeing closely with the numerical calculation for negative Δ_ρ, and also began to increase with the calculation. However, it always faltered, forming a singular triangular peak (indicating a single expected resonance). This single peak moved to increasingly higher values of Δ_ρ when for increasingly negative K/κ. Furthermore, the approximation broke down completely at $K/\kappa =$ -20.

4 Conclusion

In this investigation, we have successfully derived equations of motion and a semi-classical approximation for a Kerr non-linear resonator, and compared these to a numerical simulation written in MATLAB in the long term limit. We also demonstrated that scientifically accurate results could be obtained for simulation sizes of 25x25.

By varying K, we found that as non-linearity increased, coherence decreased, and states became increasingly mixed to a certain extent, but the number of photons in the system could not be as accurately approximated. By varying ϵ_ρ, we found that the number of photons in the oscillator increased in a nearly linear fashion as pumping strength increased. We also found that ϵ_ρ had little effect on the mixing of states. Finally, we found that as Δ_ρ changed, resonance peaks in $\langle a^\dagger a \rangle$ appeared, which varied strongly with the non-linearity of the system.

The different characteristics we have found makes it possible to develop more effective and controllable superconducting circuits. However, before doing this it is important to further explore how the semi-classical approximation breaks down for increasing K, considering a wider range of Δ_ρ, and investigating systems initially in the mixed state. The effect of varying κ on long term evolution should also be considered.

5 References

[1] John Kerr. XI. A new relation between electricity and light: Dielectrified media birefringent. *The London, Edinburgh, and Dublin Philosophical Magazine and Journal of Science*, 50(332): 337–348, 1875.

[2] Mark Dykman. Fluctuating nonlinear oscillators: from nanomechanics to quantum superconducting circuits. *I*, 2012.

[3] Gor H Hovsepyan and Gagik Yu Kryuchkyan. Excitations of photon-number states in Kerr nonlinear resonator at finite temperatures. *The European Physical Journal D*, 69(3):64, 2015. doi:10.1140/epjd/e2015-50738-y.

[4] K Grygiel and P Szlachetka. Chaos and hyperchaos in coupled Kerr oscillators. *Optics Communications*, 177(1):425–431, 2000. doi:10.1016/s0030-4018(00)00607-6.

[5] Luigi A Lugiato. II theory of optical bistability. *Progress in optics*, 21:69–216, 1984. doi:10.1016/s0079-6638(08)70122-7.

[6] Maxime Boissonneault, AC Doherty, FR Ong, P Bertet, D Vion, D Esteve, and A Blais. Backaction of a driven nonlinear resonator on a superconducting qubit. *Physical Review A*, 85(2): 022305, 2012. doi:10.1103/physreva.85.022305.

[7] Yoshitomo Okawachi, Mengjie Yu, Kevin Luke, Daniel O Carvalho, Michal Lipson, and Alexander L Gaeta. Quantum random number generator using a microresonator-based Kerr oscillator. *Optics letters*, 41(18):4194–4197, 2016. doi:10.1364/ol.41.004194.

[8] GT Foster, SL Mielke, and LA Orozco. Intensity correlations in cavity QED. *Physical Review A*, 61(5):053821, 2000. doi:10.1103/physreva.61.053821.

[9] Anna R Shahinyan, Anahit R Tamazyan, and Gagik Yu Kryuchkyan. Selective excitations of a Kerr-nonlinear resonator: exactly solvable approach. *The European Physical Journal D*, 70(6): 1–8, 2016. doi:10.1140/epjd/e2016-60707-7.

A Derivations

A.1 Semi-Classical Approximation

First, we expand Equation 2 with the commutator relation $[\hat{A}, \hat{B}] = \hat{A}\hat{B} - \hat{B}\hat{A}$ and substitute in the Hamiltonian given in Equation 1, to give

$$\begin{aligned}\dot{\rho} = &\frac{-i}{\hbar}\Big[\hbar\Delta_\rho a^\dagger a\rho + \frac{\hbar K}{2}a^\dagger a^\dagger aa\rho + i\hbar\epsilon_\rho(a^\dagger - a)\rho\Big] + \frac{i}{\hbar}\Big[\hbar\Delta_\rho\rho a^\dagger a + \frac{\hbar K}{2}\rho a^\dagger a^\dagger aa + i\hbar\epsilon_\rho\rho(a^\dagger - a)\Big] \\ &- \frac{\kappa}{2}\Big[a^\dagger a\rho - 2a\rho a^\dagger + \rho a^\dagger a\Big]\end{aligned}$$

$$= i\Delta_\rho\Big[\rho a^\dagger a - a^\dagger a\rho\Big] + \frac{iK}{2}\Big[\rho a^\dagger a^\dagger aa - a^\dagger a^\dagger aa\rho\Big] + \epsilon_\rho\Big[(a^\dagger - a)\rho - \rho(a^\dagger - a)\Big] - \frac{\kappa}{2}\Big[a^\dagger a\rho - 2a\rho a^\dagger + \rho a^\dagger a\Big]$$

$$\begin{aligned}\therefore a\dot{\rho} = &i\Delta_\rho\Big[a\rho a^\dagger a - aa^\dagger a\rho\Big] + \frac{iK}{2}\Big[a\rho a^\dagger a^\dagger aa - aa^\dagger a^\dagger aa\rho\Big] + \epsilon_\rho\Big[a(a^\dagger - a)\rho - a\rho(a^\dagger - a)\Big] \\ &- \frac{\kappa}{2}\Big[aa^\dagger a\rho - 2aa\rho a^\dagger + a\rho a^\dagger a\Big]\end{aligned}$$

From here, we use the relation $\langle A\rangle = \text{Tr}[A\rho]$ to allow us to calculate $\langle\dot{\rho}\rangle$. We also use the relation $\text{Tr}[A + B + C] = \text{Tr}[A] + \text{Tr}[B] + \text{Tr}[C]$ to allow us to look at each element of this equation individually.

$$\begin{aligned}\langle\dot{a}\rangle = \text{Tr}[a\dot{\rho}] = i\Delta_\rho &\overbrace{\text{Tr}\Big[a\rho a^\dagger a - aa^\dagger a\rho\Big]}^{\text{(A)}} + \frac{iK}{2}\overbrace{\text{Tr}\Big[a\rho a^\dagger a^\dagger aa - aa^\dagger a^\dagger aa\rho\Big]}^{\text{(B)}} \\ &+ \epsilon_\rho\underbrace{\text{Tr}\Big[a(a^\dagger - a)\rho - a\rho(a^\dagger - a)\Big]}_{\text{(C)}} - \frac{\kappa}{2}\underbrace{\text{Tr}\Big[aa^\dagger a\rho - 2aa\rho a^\dagger + a\rho a^\dagger a\Big]}_{\text{(D)}}\end{aligned}$$

When considering each element of the equation, we will use the cyclic nature of the trace operation, $\text{Tr}[ABC] = \text{Tr}[CAB] = \text{Tr}[BCA]$, the relation $\text{Tr}[AB] = -\text{Tr}[BA]$, and the definition $[a, a^\dagger] = 1$. For (B), we also apply the relation $[A, BC] = [A, B]C + B[A, C]$.

$$\begin{aligned}\text{(A)} &= \text{Tr}[a\rho a^\dagger a] - \text{Tr}[aa^\dagger a\rho] = \text{Tr}[a^\dagger aa\rho] - \text{Tr}[aa^\dagger a\rho] \\ &= \text{Tr}\left[(a^\dagger a - aa^\dagger)a\rho\right] = \text{Tr}\left[[a^\dagger, a]a\rho\right] = \text{Tr}[-a\rho] \\ &= -\langle a\rangle\end{aligned}$$

$$\begin{aligned}\text{(B)} &= \text{Tr}[a\rho a^\dagger a^\dagger aa] - \text{Tr}[aa^\dagger a^\dagger aa\rho] = \text{Tr}[a^\dagger a^\dagger aaa\rho] - \text{Tr}[aa^\dagger a^\dagger aa\rho] \\ &= \text{Tr}[a^\dagger a^\dagger aaa\rho - aa^\dagger a^\dagger aa\rho] = \text{Tr}\left[(a^\dagger a^\dagger a - aa^\dagger a^\dagger)aa\rho\right] \\ &= \text{Tr}\left[[a^\dagger a^\dagger, a]aa\rho\right] = -\text{Tr}\Big[\big([a, a^\dagger]a^\dagger + a^\dagger[a, a^\dagger]\big)aa\rho\Big] = -2\,\text{Tr}[a^\dagger aa\rho] \\ &= -2\langle a^\dagger aa\rangle\end{aligned}$$

$$\begin{aligned}
\text{C} &= \mathrm{Tr}\left[a(a^\dagger - a)\rho\right] - \mathrm{Tr}\left[a\rho(a^\dagger - a)\right] = \mathrm{Tr}[aa^\dagger\rho] - \mathrm{Tr}[aa\rho] - \mathrm{Tr}[a\rho a^\dagger] + \mathrm{Tr}[a\rho a] \\
&= \mathrm{Tr}[aa^\dagger\rho] - \mathrm{Tr}[aa\rho] - \mathrm{Tr}[a^\dagger a\rho] + \mathrm{Tr}[aa\rho] = \mathrm{Tr}[aa^\dagger\rho - a^\dagger a\rho] \\
&= \mathrm{Tr}\left[(aa^\dagger - a^\dagger a)\rho\right] = \mathrm{Tr}\left[[a, a^\dagger]\rho\right] = \mathrm{Tr}[\rho] \\
&= 1
\end{aligned}$$

$$\begin{aligned}
\text{D} &= \mathrm{Tr}[aa^\dagger a\rho] - 2\,\mathrm{Tr}[aa\rho a^\dagger] + \mathrm{Tr}[a\rho a^\dagger a] = \mathrm{Tr}[aa^\dagger a\rho] - 2\,\mathrm{Tr}[a^\dagger aa\rho] + \mathrm{Tr}[a^\dagger aa\rho] \\
&= \mathrm{Tr}[aa^\dagger a\rho - a^\dagger aa\rho] = \mathrm{Tr}\left[(aa^\dagger - a^\dagger a)a\rho\right] \\
&= \mathrm{Tr}\left[[a, a^\dagger]a\rho\right] = \mathrm{Tr}[a\rho] \\
&= \langle a \rangle
\end{aligned}$$

We can then combine these sections together to give Equation 3, the equation of motion of $\langle a \rangle$

$$\begin{aligned}
\langle \dot{a} \rangle &= i\Delta_\rho\,\text{A} + \frac{iK}{2}\,\text{B} + \epsilon_\rho\,\text{C} - \frac{\kappa}{2}\,\text{D} \\
&= -i\Delta_\rho\langle a \rangle - iK\langle a^\dagger aa \rangle + \epsilon_\rho - \frac{\kappa}{2}\langle a \rangle.
\end{aligned}$$

From here, we can let the time derivative, $\langle \dot{a} \rangle = 0$ and define a new complex amplitude $\langle a \rangle = \alpha$. After rearranging, we arrive at the equation

$$iK|\alpha|^2\alpha + \left(i\Delta_\rho + \frac{\kappa}{2}\right)\alpha - \epsilon_\rho = 0$$

A.2 Cubic Equation

By rearranging for α and multiplying by its complex conjugate, we find

$$\begin{aligned}
\alpha &= \frac{\epsilon_\rho}{\frac{\kappa}{2} + iK|\alpha|^2 + i\Delta_\rho} \\
\alpha^* &= \frac{\epsilon_\rho}{\frac{\kappa}{2} - iK|\alpha|^2 - i\Delta_\rho} \\
|\alpha|^2 = \alpha\alpha^* &= \frac{\epsilon_\rho^2}{\left[\frac{\kappa}{2} + iK|\alpha|^2 + i\Delta_\rho\right]\left[\frac{\kappa}{2} - iK|\alpha|^2 - i\Delta_\rho\right]} \\
&= \frac{\epsilon_\rho^2}{K^2|\alpha|^4 + 2K\Delta_\rho|\alpha|^2 + \frac{\kappa^2}{4} + \Delta_\rho^2}
\end{aligned}$$

We therefore arrive at an equation cubic in $|\alpha|^2$, Equation 4

$$K^2|\alpha|^6 + 2K\Delta_\rho|\alpha|^4 + \left(\frac{\kappa^2}{4} + \Delta_\rho^2\right)|\alpha|^2 - \epsilon_\rho^2 = 0$$

A.3 Coupled Equations of Motion

To obtain the coupled equation of motion shown in Equation 5, we first expand Equation 2 as done in Appendix A.1, before acting on the left with $\langle n|$ and the right with $|n\rangle$. This gives the equation

$$\langle n|\dot{\rho}|n'\rangle = i\Delta_\rho\Big[\overbrace{\langle n|\rho a^\dagger a|n'\rangle}^{\text{A}} - \overbrace{\langle n|a^\dagger a\rho|n'\rangle}^{\text{B}}\Big] + \frac{iK}{2}\Big[\overbrace{\langle n|\rho a^\dagger a^\dagger aa|n'\rangle}^{\text{C}} - \overbrace{\langle n|a^\dagger a^\dagger aa\rho|n'\rangle}^{\text{D}}\Big] + \epsilon_\rho\Big[\overbrace{\langle n|a^\dagger\rho|n'\rangle}^{\text{E}} - \overbrace{\langle n|a\rho|n'\rangle}^{\text{F}} - \underbrace{\langle n|\rho a^\dagger|n'\rangle}_{\text{G}} - \underbrace{\langle n|\rho a|n'\rangle}_{\text{H}}\Big] - \frac{\kappa}{2}\Big[\underbrace{\langle n|a^\dagger a\rho|n'\rangle}_{\text{I}} - \underbrace{2\langle n|a\rho a^\dagger|n'\rangle}_{\text{J}} + \underbrace{\langle n|\rho a^\dagger a|n'\rangle}_{\text{K}}\Big]$$

After splitting the equation into parts, we use the definition of the raising and lowering operators, $a^\dagger|n\rangle = \sqrt{n+1}|n+1\rangle$ and $a|n\rangle = \sqrt{n}|n-1\rangle$. We also use the fact that $[AB|\phi\rangle] = [\langle\phi|B^\dagger A^\dagger]^*$, and $n = n^*$ as n and n' are real.

$$\begin{aligned}\text{A} &= \langle n|\rho a^\dagger a|n'\rangle = \sqrt{n'}\langle n|\rho a^\dagger|n'-1\rangle \\ &= n'\langle n|\rho|n'\rangle\end{aligned}$$

$$\begin{aligned}\text{B} &= \langle n|a^\dagger a\rho|n'\rangle = \big[a^\dagger a|n\rangle\big]^*\rho|n'\rangle = \big[\sqrt{n}a^\dagger|n-1\rangle\big]^*\rho|n'\rangle = \big[n|n\rangle\big]^*\rho|n'\rangle \\ &= n\langle n|\rho|n'\rangle\end{aligned}$$

$$\begin{aligned}\text{C} &= \langle n|\rho a^\dagger a^\dagger aa|n'\rangle = \sqrt{n'}\langle n|\rho a^\dagger a^\dagger a|n'-1\rangle = \sqrt{n'}\sqrt{n'-1}\langle n|\rho a^\dagger a^\dagger|n'-2\rangle = \sqrt{n'}(n'-1)\langle n|\rho a^\dagger|n'-1\rangle \\ &= n'(n'-1)\langle n|\rho a|n'\rangle\end{aligned}$$

$$\begin{aligned}\text{D} &= \langle n|a^\dagger a^\dagger aa\rho|n'\rangle = \big[a^\dagger a^\dagger aa|n\rangle\big]^*\rho|n'\rangle = \big[\sqrt{n}a^\dagger a^\dagger a|n-1\rangle\big]^*\rho|n'\rangle = \big[\sqrt{n}\sqrt{n-1}a^\dagger a^\dagger|n-2\rangle\big]^*\rho|n'\rangle \\ &= \big[\sqrt{n}(n-1)a^\dagger|n-1\rangle\big]^*\rho|n'\rangle = \big[n(n-1)|n\rangle\big]^*\rho|n'\rangle \\ &= n(n-1)\langle n|\rho a|n'\rangle\end{aligned}$$

$$\begin{aligned}\text{E} &= \langle n|a^\dagger\rho|n'\rangle = \big[a|n\rangle\big]^*\rho|n'\rangle = \big[\sqrt{n}|n-1\rangle\big]^*\rho|n'\rangle \\ &= \sqrt{n}\langle n-1|\rho|n'\rangle\end{aligned}$$

$$\begin{aligned}\text{F} &= \langle n|a\rho|n'\rangle = \big[a^\dagger|n\rangle\big]^*\rho|n'\rangle = \big[\sqrt{n+1}|n+11\rangle\big]^*\rho|n'\rangle \\ &= \sqrt{n+1}\langle n+1|\rho|n'\rangle\end{aligned}$$

$$\begin{aligned}\text{G} &= \langle n|\rho a^\dagger|n'\rangle \\ &= \sqrt{n'+1}\langle n|\rho a^\dagger|n'+1\rangle\end{aligned}$$

$$\begin{aligned}\text{H} &= \langle n|\rho a|n'\rangle \\ &= \sqrt{n'}\langle n|\rho a^\dagger|n'-1\rangle\end{aligned}$$

$$\begin{aligned}(\mathsf{I}) &= \langle n|a^\dagger a\rho|n'\rangle = \big[a^\dagger a|n\rangle\big]^*\rho|n'\rangle = \big[\sqrt{n}a^\dagger|n-1\rangle\big]^*\rho|n'\rangle = \big[n|n\rangle\big]^*\rho|n'\rangle \\ &= n\langle n|\rho|n'\rangle\end{aligned}$$

$$\begin{aligned}(\mathsf{J}) &= 2\langle n|a\rho a^\dagger|n'\rangle = 2\big[a^\dagger|n\rangle\big]^*\rho a^\dagger|n'\rangle = 2\big[\sqrt{n+1}|n+1\rangle\big]^*\rho\sqrt{n'+1}|n'+1\rangle \\ &= 2\sqrt{n+1}\sqrt{n'+1}\langle n+1|\rho|n'+1\rangle\end{aligned}$$

$$\begin{aligned}(\mathsf{K}) &= \langle n|\rho a^\dagger a|n'\rangle = \sqrt{n'}\langle n|\rho a^\dagger|n'-1\rangle \\ &= n'\langle n|\rho|n'\rangle\end{aligned}$$

After recombining these sections we therefore find

$$\begin{aligned}\langle n|\dot{\rho}|n'\rangle = {} & i\Delta_\rho n'\langle n|\rho|n'\rangle - i\Delta_\rho n\langle n|\rho|n'\rangle + \frac{iK}{2}n'(n'-1)\langle n|\rho|n'\rangle - \frac{iK}{2}n(n-1)\langle n|\rho|n'\rangle \\ & + \epsilon_\rho\sqrt{n}\langle n-1|\rho|n'\rangle - \epsilon_\rho\sqrt{n+1}\langle n+1|\rho|n'\rangle - \epsilon_\rho\sqrt{n'+1}\langle n|\rho|n'+1\rangle + \epsilon_\rho\sqrt{n'-1}\langle n|\rho|n'\rangle \\ & - \frac{\kappa}{2}n\sqrt{n}\langle n|\rho|n'\rangle + \kappa\sqrt{n+1}\sqrt{n'+1}\sqrt{n}\langle n+1|\rho|n'+1\rangle - \frac{\kappa}{2}n'\sqrt{n}\langle n|\rho|n'\rangle\end{aligned}$$

By writing the density operator in terms of the number states, n and n', $\rho(t) = \sum_{n'=0}^{\infty}\sum_{n=0}^{\infty}\rho_{nn'}|n\rangle\langle n'|$ where we define $\rho_{nn'}(t) = \langle n|\rho(t)|n'\rangle$. Because the number states are orthonormal, we therefore find Equation 5, the set of coupled equations of motion for the density matrix elements, to be

$$\begin{aligned}\dot{\rho}_{n,n'}(t) = \langle n|\dot{\rho}|n'\rangle = {} & \rho_{n,n'}(t)\Big[i\Delta_\rho(n'-n) + \frac{iK}{2}\big(n'(n'-1) - n(n-1)\big) - \frac{\kappa}{2}(n+n')\Big] \\ & + \rho_{n-1,n'}(t)\Big[\epsilon_\rho\sqrt{n}\Big] - \rho_{n+1,n'}(t)\Big[\epsilon_\rho\sqrt{n+1}\Big] \\ & + \rho_{n,n'-1}(t)\Big[\epsilon_\rho\sqrt{n'}\Big] - \rho_{n,n'+1}(t)\Big[\epsilon_\rho\sqrt{n'+1}\Big] \\ & + \rho_{n+1,n'+1}(t)\Big[\kappa\sqrt{n+1}\sqrt{n'+1}\Big].\end{aligned}$$

B Code

B.1 Integration

```
%% Oli Gordon & Matthew Edmondson QCD Project
clearvars
close all

%% Settings
maxsize = 25;                       % Grid size
startn = 0;                         % Starting points
startn_ = 0;

maxtime = 15;                       % Maximum time
ode_inc = 1;                        % Timestep for ODE to calculate over
odesteps = 100;                     % Number of calculations per ODE
saving = 0;                         % Choose to save 0|1 (no|yes)

K = -0.5;                           % Other variables
dp = 0;
ep = 1;
kappa = 1;

%% Setup
timesteps = maxtime/ode_inc;

% Preallocate arrays, including +2 of padding
p_pad = zeros(maxsize+2,maxsize+2);
pdot_pad = zeros(maxsize+2,maxsize+2);
traces = zeros(1,(odesteps*maxtime)+1);
traces2 = zeros(1,(odesteps*maxtime)+1);
adag_a = zeros(1,(odesteps*maxtime)+1);
g20 = zeros(1,(odesteps*maxtime)+1);
amp = zeros(1,(odesteps*maxtime)+1);
timeaxis_calc = 0:ode_inc:(ode_inc*timesteps);
timeaxis_plot = zeros(1,(odesteps*maxtime)+1);
timeaxis_plot(end) = maxtime;

% Calculate raising and lowering operators in matrix form
a = diag(sqrt(1:maxsize-1),1);
a_dag = diag(sqrt(1:maxsize-1),-1);

% Create list of <n,n'> to call through
row = 0:maxsize-1;
col = 0:maxsize-1;
[X,Y] = meshgrid(row,col);
nall = reshape(Y,[1,maxsize^2]);
n_all = reshape(X,[1,maxsize^2]);

% Create and explore initial p
p_pad(startn_+2,startn+2) = 1;
p = p_pad(2:end-1,2:end-1);

%% Main Calculations
% Split calls of the ODE into parts, limiting matrix size to save RAM and
% therefore allow us to investigate longer timescales and higher
% resolutions :)
for timers = 1:timesteps
```

```
55      %% Integration
56      % Determine time period ODE is performed over
57      tspan = timeaxis_calc(timers):ode_inc/odesteps:...
58          timeaxis_calc(timers+1);
59
60      % Perform ODE
61      p = reshape(p,[1,maxsize^2]);
62      [t,p_new] = ode45(@(t,p) ...
63          p_dot_cal(p,maxsize,nall,n_all,dp,ep,K,kappa),tspan, p);
64
65      % Store outputs of ODE
66      timeaxis_plot((((timers-1)*odesteps)+1):(((timers)*odesteps))) ...
67          = t(1:end-1);
68
69      %% Calculations
70      for diag_loop = 1:size(p_new,1)-1
71          % p (should be =1), p^2 (0-1, expect to decrease over time)
72          p_segment = reshape(p_new(diag_loop,:),[maxsize,maxsize])';
73          traces(((timers-1)*odesteps)+diag_loop) = ...
74              sum(diag(p_segment));
75          traces2(((timers-1)*odesteps)+diag_loop) = ...
76              sum(diag((p_segment^2)));
77          adag_a(((timers-1)*odesteps)+diag_loop) = ...
78              sum(diag(a_dag*a*p_segment));
79          g20(((timers-1)*odesteps)+diag_loop) = ...
80              sum(diag((a_dag*a_dag*a*a*p_segment)/...
81              (adag_a(((timers-1)*odesteps)+diag_loop))^2));
82          amp(((timers-1)*odesteps)+diag_loop) = ...
83              sum(diag(a*p_segment));
84      end
85
86      % Reshape last value of p to a 2D matrix for the next time around
87      p = reshape(p_new(end,:),[maxsize,maxsize])';
88
89  end
90
91  % Get calculations for very last result
92  traces(end) = sum(diag(p));
93  traces2(end) = sum(diag((p^2)));
94  adag_a(end) = sum(diag(a_dag*a*p));
95  g20(end) = sum(diag(a_dag*a_dag*a*a*p))/((adag_a(end))^2);
96  amp(end) = sum(diag(a*p));
97
98  % Make semiclassical approximation
99  A = K^2;
100 B = 2*dp*K;
101 C = (kappa^2)/4 + dp^2;
102 D = -(ep^2);
103 p = [A B C D];
104 semiclass_all = roots(p);
105 [~, idx] = sort(abs(imag(semiclass_all)));
106 semiclass_sorted = semiclass_all(idx);
107 semiclass = real(semiclass_sorted(1));
108
109 %% Plot Graphs
110 set(0,'defaulttextInterpreter','latex');
111
112 % Plot Figures
113 figure()
114 subplot(2,2,1)
```

```
plot(timeaxis_plot,abs(traces))
ylim([0,1.2])
xlabel('Time (s)')
ylabel('Tr$[\rho]$')
%set(gca,'fontsize',12)

subplot(2,2,2)
plot(timeaxis_plot,abs(traces2))
ylim([0,1.2])
xlabel('Time (s)')
ylabel('Tr$[\rho^2]$')
%set(gca,'fontsize',12)

subplot(2,2,3)
hold on
plot(timeaxis_plot,abs(adag_a))
plot(timeaxis_plot,semiclass.*ones(1,length(timeaxis_plot)),'r--')
xlabel('Time (s)')
ylabel('$\langle a^\dagger a\rangle$','FontSize',12)
legend({'Numerical Integration';'Semi-Classical Approximation'},...
    'Location','best')
set(gca,'fontsize',12)

subplot(2,2,4)
plot(timeaxis_plot,abs(g20))
xlabel('Time (s)')
ylabel(['$\frac{\langle a^\dagger a^\dagger aa \rangle}'...
    '{{\langle a^\dagger a \rangle}^2}$ '],'FontSize',16)
ylim([0 inf])
%set(gca,'fontsize',12)

% subplot(2,3,5)
% plot(timeaxis_plot,abs(amp))
% xlabel('Time (Arbitrary Units)')
% ylabel('$\langle a\rangle$','FontSize',12)


set(0,'defaulttextInterpreter','tex');

% Save Output
if saving == 1
    save(['Data/Outputs_K=',num2str(K),'_dp=',num2str(dp),...
        '_ep=',num2str(ep),'_kappa=',num2str(kappa),'.mat'],...
        'traces','traces2','adag_a','g20','timeaxis_plot','semiclass')
end
```

```
function [pdot] = p_dot_cal(p_1d,maxsize,nall,n_all,dp,ep,K,kappa)

% Set up arrays
pdot_pad = zeros(maxsize+2,maxsize+2);

p = reshape(p_1d,[maxsize,maxsize]);
p_pad = padarray(p,[1,1]);

% For all n,n'
for posi = 1:maxsize^2
    % Extract position
    n = nall(posi);
```

```
    n_ = n_all(posi);

    % Calculate pdot from equation
    pdot_pad(n+2,n_+2) = (p_pad(n+2,n_+2))*( (1i * dp * (n_ - n))...
        + 1i * K/2 * (n_ *(n_ -1) - n * (n-1)) - 0.5*kappa * (n + n_)) ...
        + p_pad(n+3,n_+3)*( kappa*sqrt(n+1)*sqrt(n_+1))...
        + (p_pad(n+1,n_+2)*( ep*sqrt(n)))...
        - p_pad(n+3,n_+2)*( ep*sqrt(n+1))...
        - p_pad(n+2,n_+3)*( ep*sqrt(n_+1))...
        +p_pad(n+2,n_+1)*( ep*sqrt(n_));
end

% Strip padding
pdot = pdot_pad(2:end-1,2:end-1);
pdot = reshape(pdot,[maxsize^2,1]);
end
```

B.2 Long-Term Behaviour

```
%% Oli Gordon & Matthew Edmondson QCD Project
clearvars
close all
set(0,'defaulttextInterpreter','latex');

%% Settings

% Pick thing to vary
varying = 'ep';
in_range = 20:-0.2:-0;

% Pick other constants
dp = 0;
ep = 1;
kappa = 1;
K = -0.5;

% Preallocate matrices
trace_long = zeros(1,length(in_range));
trace2_long = zeros(1,length(in_range));
adag_a_long = zeros(1,length(in_range));
g20_long = zeros(1,length(in_range));
in_leg = cellstr(num2str(in_range'))';

%% Plot
hold all
for in_loop = 1:length(in_range)
    % Read in
    assignin('base',varying,in_range(in_loop))
    filename = ['Data/Outputs_K=',num2str(K),'_dp=',num2str(dp),...
        '_ep=',num2str(ep),'_kappa=',num2str(kappa),'.mat'];
    load(filename);

    % Store in vectors
    trace_long(in_loop) = abs(traces(end));
    trace2_long(in_loop) = abs(traces2(end));
    adag_a_long(in_loop) = abs(adag_a(end));
    g20_long(in_loop) = abs(g20(end));

    % Add to plot
    figure(1)
    hold all
    plot(timeaxis_plot,abs(traces))
    figure(2)
    hold all
    plot(timeaxis_plot,abs(traces2))
    figure(3)
    hold all
    plot(timeaxis_plot,abs(adag_a))
    figure(4)
    hold all
    plot(timeaxis_plot,abs(g20))
end

%% Niceties

```

```
set(0,'defaulttextInterpreter','latex');

if strcmp(varying,'K') == 1
    varying_lgd = 'K';
elseif strcmp(varying,'dp') == 1
    varying_lgd = '\Delta_\rho';
elseif strcmp(varying,'ep') == 1
    varying_lgd = '\epsilon_\rho';
elseif strcmp(varying,'kappa') == 1
    varying_lgd = '\kappa';
end

% Plot Tr[p]
figure(1)
lg1 = legend(in_leg);
title(lg1,varying_lgd)
xlabel('Time (Arbitrary Units)')
ylabel('Tr$[\rho]$')
ylim([0,1.2])

% Plot Tr[p^2]
figure(2)
lg2 = legend(in_leg);
title(lg2,varying_lgd)
xlabel('Time (Arbitrary Units)')
ylabel('Tr$[\rho^2]$')
ylim([0,1.2])

% Plot Tr[adag a]
figure(3)
lg3 = legend(in_leg);
title(lg3,varying_lgd)
xlabel('Time (Arbitrary Units)')
ylabel('$\langle a^\dagger a\rangle$','FontSize',12)

% Plot Tr[g^2]
figure(4)
lg4 = legend(in_leg);
title(lg4,varying_lgd)
xlabel('Time (Arbitrary Units)')
ylabel(['$\frac{\langle a^\dagger a^\dagger aa \rangle}{'...
    '{\langle a^\dagger a \rangle}^2}$ '],'FontSize',16)

% Plot long term behaviors
figure(5)
subplot(2,2,1)
plot(in_range,trace_long)
xlabel(varying_lgd,'Interpreter','tex')
ylabel('Tr$[\rho]$')
ylim([0,1.2])

subplot(2,2,2)
plot(in_range,trace2_long)
xlabel(varying_lgd,'Interpreter','tex')
ylabel('Tr$[\rho^2]$')
ylim([0,1.2])

subplot(2,2,3)
plot(in_range,adag_a_long)
xlabel(varying_lgd,'Interpreter','tex')
```

```
117 ylabel('$\langle a^\dagger a\rangle$','FontSize',12)
118
119 subplot(2,2,4)
120 plot(in_range,g20_long)
121 xlabel(varying_lgd,'Interpreter','tex')
122 ylabel(['$\frac{\langle a^\dagger a^\dagger aa \rangle}'...
123     '{{\langle a^\dagger a \rangle}^2}$ '],'FontSize',16)
124
125
126 % Save figures
127 figs = [figure(1),figure(2),figure(3),figure(4)];
128 %savefig(figs,'Data/K_vary')
129
130 set(0,'defaulttextInterpreter','tex');
```